Available online at www.sciencedirect.com
SCIENCE DIRECT®
Journal of Solid State Chemistry 178 (2005) 680–687
JOURNAL OF SOLID STATE CHEMISTRY
www.elsevier.com/locate/jssc

The Al^{3+} stabilized phase $Li_{3-3x}Al_xBO_3$

M. He[a,b,*], H. Okudera[a], J. Fleig[a], A. Simon[a], X.L. Chen[b], J. Maier[a]

[a] *Max Planck Institute for Solid State Research, Heisenbergstrasse 1, D-70569 Stuttgart, Germany*
[b] *Institute of Physics, Chinese Academy of Sciences, P.O. Box 603, 100080 Beijing, China*

Received 4 November 2004; received in revised form 8 December 2004; accepted 11 December 2004

Abstract

The structure of an Al^{3+} stabilized phase $Li_{3-3x}Al_xBO_3$ ($x \approx 0.18$) was determined by means of single crystal X-ray diffraction. This phase crystallizes in space group $P6_122$ or $P6_522$, with lattice constants $a = 4.9019(5)$ Å, $c = 17.538(2)$ Å and $Z = 6$. The unit cell consists of six layers of BO_3 groups with Li^+ cations distributing statistically on five crystallographic sites, none of which is fully occupied. The Li sites are close to each other and a three-dimensional network results when Li sites only within 1.65 Å are connected. Significant ionic conductivity was observed for this phase.

Keywords: Borate; Crystal structure; Ionic conductivity

1. Introduction

α Li_3BO_3 was first reported by Rollet and Bouaziz [1] and gained general interest after Shannon et al. [2] had found that introducing Li^+ vacancies by substitution of C for B in this structure would lead to significant Li ionic conduction. In 1960, Lehmann and Wöckel [3] reported a high-temperature phase (β phase) of Li_3BO_3, which could not be retained on quenching. The structure of α Li_3BO_3 was determined by Stewner [4] in 1971, and in the same paper, a monoclinic unit cell was suggested for the β phase.

In our previous study on the Li_2O–Al_2O_3–B_2O_3 system [5], we found a new phase with a composition close to $0.66Li_2O \cdot 0.06Al_2O_3 \cdot 0.28B_2O_3$. Its powder pattern could be indexed with a hexagonal unit cell yielding a high figure of merit. Later, compounds with very similar powder patterns were also observed in Li_2O–MgO–B_2O_3 [6] and Li_2O–CaO–B_2O_3 [7] systems. Because of the small amounts of Al^{3+}, Mg^{2+} and Ca^{2+} in these compounds, they have been supposed to represent the high temperature phase of Li_3BO_3 [7]. However, further detailed study is necessary to confirm this assumption.

In this study, one of these unknown phases, $0.66Li_2O \cdot 0.06Al_2O_3 \cdot 0.28B_2O_3$, is solved with single crystal technique. It was confirmed that this compound is in fact a new phase with a stoichiometric composition. Li^+ ions distribute at several different crystallographic positions, none of which is fully occupied. Because of so many vacancies available in this structure, and also because of the short distances between these positions, good ionic conductivity is expected and experimentally verified for this compound.

2. Experimental

Starting materials with a composition $0.66Li_2CO_3 \cdot 0.06Al_2O_3 \cdot 0.56H_3BO_3$ were thoroughly mixed, ground in an agate mortar and then sintered at 620 °C for 12 days in an electrical furnace to get the desired

*Corresponding author. Max Planck Institute for Solid State Research, Abteilung Simon, Heisenbergstrasse 1, D-70569 Stuttgart, Germany. Fax: +49 711 689 1091.
E-mail address: m.he@fkf.mpg.de (M. He).

0022-4596/$ - see front matter © 2004 Elsevier Inc. All rights reserved.
doi:10.1016/j.jssc.2004.12.017

phase. Single crystals large enough for X-ray measurement could be selected from the polycrystalline product.

Single-crystal diffraction intensities were collected with a Stoe IPDS system. More details can be found in Table 1. The program Shelxtl [8] was used to solve and refine the structure. Platon [9] was used to find missing symmetry of the structure model.

Powder X-ray diffraction data were also collected using a Stoe Stadi powder diffraction system equipped with an incident beam curved germanium monochromator. Data were collected in Debye-Scherrer geometry with a small linear PSD (2θ range 4°).

A polycrystalline sample was further ground and cold-pressed into a pellet of 10 mm diameter and 1.25 mm thickness for ionic conductivity measurement, the density of which is calculated to be around 79% of the theoretical value with reference to the structure solution. Au-electrodes were evaporated onto the pellet, and additional Pt paste was used to ensure good electrode contacts. The ionic conductivity was investigated by impedance spectroscopy (Solartron FRA 1260) in the frequency range from 1 Hz to 1 MHz.

Table 1
Crystal data and details of the structure determination for $Li_{2.46}Al_{0.18}BO_3$

Crystal data	
$Li_{2.46}Al_{0.18}BO_3$	Mo$K\alpha$ radiation
$Mr = 80.74$	Cell parameters from 5285 reflections
Hexagonal, $P6_122$ (No.178)	$\theta = 3.49-31.97°$
$a = 4.9019(5)$ Å	$\mu = 0.248\,mm^{-1}$
$c = 17.538(2)$ Å	$T = 293(2)$ K
$V = 364.96(7)$ Å^3	Plate, colorless
$Z = 6$	$0.125 \times 0.120 \times 0.040$ mm
$D_x = 2.204\,Mg\,m^{-3}$	
Data collection	
Stoe IPDS II diffractometer	404 reflections with $>2\sigma(I)$
ω scan	$R_{int} = 0.0411$, $R_\sigma = 0.0146$
Absorption correction: numerical	$\theta_{min} = 4.80$, $\theta_{max} = 32.03°$
$T_{min} = 0.9789$, $T_{max} = 0.9924$	$h = -7 \rightarrow 7$
4533 measured reflections	$k = -7 \rightarrow 7$
433 independent reflections	$l = -26 \rightarrow 26$
Refinement	
Refinement on F^2	
$R[F^2 > 2\sigma(F^2)] = 0.0518$	$\omega = 1/[\sigma^2(F_o^2) + (0.0174P)^2 + 0.3963P]$ where $P = (F_o^2 + 2F_c^2)/3$
$wR(F^2) = 0.1192$	
$S = 1.338$	$(\Delta/\sigma)_{max} = 0.000$
433 reflections	$\Delta\rho_{max} = 0.244\,e$Å^{-3}
47 parameters	$\Delta\rho_{min} = -0.304\,e$Å^{-3}

3. Results and discussion

3.1. Structure solution

A one-dimensional projection of single crystal data and an experimental powder pattern of the sample are shown in Fig. 1. The good agreement between them indicates that the single crystal specimen represents the entire product.

Because of only a small amount of Al_2O_3 in the starting materials, the structure was first solved as Li_3BO_3. Reflection conditions ($00l$: $l = 6n$) lead to two pairs of enantiomorphic space groups, $P6_1$ and $P6_5$, or $P6_122$ and $P6_522$ as candidates of possible space groups. The number of formula units per cell (Z) was assumed to be 6 according to cell volume and space group.

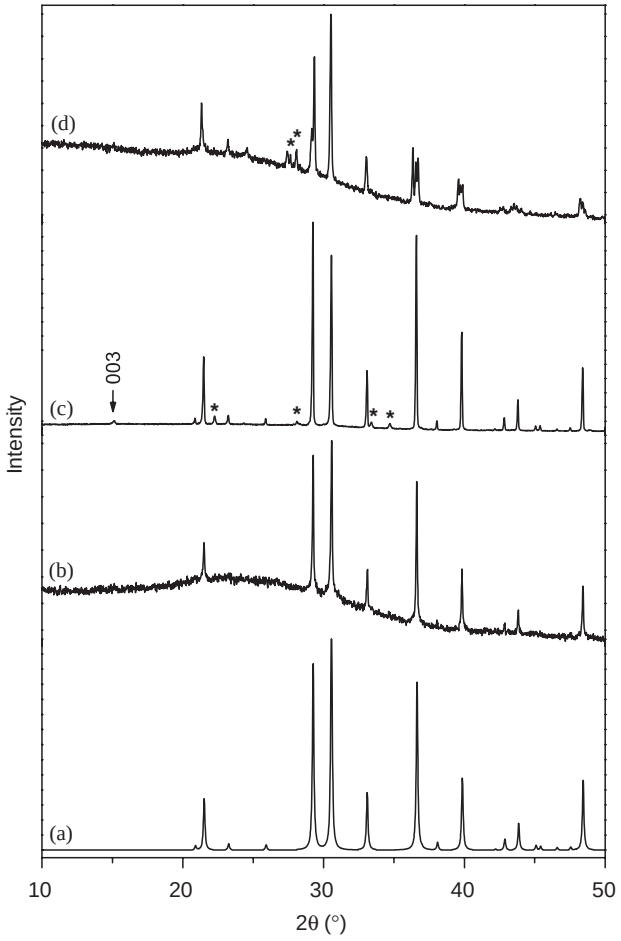

Fig. 1. One-dimensional projection of single crystal data (a) and experimental powder diffraction pattern (b) (Cu$K\alpha_1$, 70 s/0.1° in 2θ) of $Li_{3-3x}Al_xBO_3$ ($x \approx 0.18$). Profiles c and d were collected on samples prepared under slightly different conditions (see Section 3.5). The 2θ scale of the projection of single crystal data has been adjusted to compare with the experimental powder patterns directly. Peaks marked with * result from impurities, γ $LiAlO_2$ (in c) and β $Li_4B_2O_5$ (in d).

At first, the structure was solved in $P6_1$. Application of direct methods revealed all the B, O and two Li positions. However, program Platon [9] suggested the presence of two-fold axes, and the structure solution was restarted in space group $P6_122$. One B site (at 6*a*), two O sites (O1 at 12*c*, O2 at 6*a*) and one Li position (at 12*c*) could be easily found, and no significant peaks showed up in the difference Fourier map. The highest peak (0.72 e/Å^3) at 6*b* position might indicate an additional Li atom, and the bond valences are calculated for this position with Brown and Altermatt's parameters [10]. The results of the calculation are presented in Table 2. All the bond lengths are quite reasonable, and so are the bond valence sums, indicating that the residual density at this position could be attributed to partial occupation by Li atoms. The site occupation factor (sof) of this position (Li2) was refined to be only about 0.15, indicating that there should be further Li positions not revealed yet.

Table 2
Interatomic distances and bond valences with Li2 at $x = 0.0859$, $y = 0.1718$, $z = 0.75$ as revealed by difference Fourier map

Atom1	Atom2	Distance (Å)	Bond valence *s*
Li1	O1	1.888	0.320
	O2	1.907	0.304
	O1	1.927	0.288
	O1	2.005	0.233
ΣS (Li1) = 1.145			
B	O2	1.377	0.984
	O1 × 2	1.387	0.958
ΣS (B) = 2.900			
O1	B	1.387	0.958
	Li1	1.888	0.320
	Li1	1.927	0.288
	Li1	2.005	0.233
	Li2	2.03	0.218
ΣS (O1) = 2.017			
O2	B	1.377	0.984
	Li1 × 2	1.907	0.304
	Li2 × 2	2.00	0.236
ΣS (O2) = 2.064			
Li2	O2 × 2	2.03	0.218
	O1 × 2	2.00	0.236
ΣS (Li2) = 0.908			
Shortest distances between cations			
Li1	Li1	2.447	
	Li2	1.98	
	B	2.808	
Li2	Li1	1.98	
	Li2	3.01	
	B	2.68	

Note: The positions of other atoms at this stage are as follows: Li1 (0.0044, 0.3294, 0.0330), B (0.3221, 0, 0), O1 (0.0449, 0.7305, 0.0202), O2 (0.6030, 0, 0). The formula ($s = \exp[-(r-r_0)/B]$) and parameters (B = 0.37, $r_0$1.466 and 1.371 for Li^+ and B^{3+}, respectively) to calculate bond valences are cited from [10].

The structure refinement, difference Fourier syntheses and bond valence calculations were repeatedly made to explore other Li^+ sites, and finally three more Li sites (Li3–Li5) were found. However, the distances among all the five Li sites are so short that none of them can be fully occupied. When the sof's of all the five Li sites were allowed to vary without any constraints, they were refined to 1.18, 0.23, 0.25, 0.11, and 0.10 for Li1 to Li5, respectively. This corresponds to 20.46 Li^+ in a unit cell, which is little larger than the expected value (18 Li^+). Obviously, the sof of Li1 is meaningless. Moreover, if Li1 is fully occupied, Li3, Li4 and Li5 sites cannot be occupied because of the very short Li–Li distances. Now Al^{3+} has to be taken into account. The rather regular tetrahedral coordination, the short average Li–O distances and the greater-than-one sof of the Li1 site suggest that this site is partially occupied by Al^{3+}. When the partial occupation of Al^{3+} on the Li1 position was involved in the refinement, which was subject to a constraint to make the sum of all charges of Li^+ and Al^{3+} cations 18 in a unit cell, the sof of Al^{3+}, and Li1 to Li5 were refined to 0.09, 0.70, 0.23, 0.25, 0.11, and 0.10, respectively. This leads to a formula $Li_{2.4(3)}Al_{0.18(4)}BO_3$, which is in good agreement with the composition of the starting materials. The formula is written as

Table 3
Fractional atomic coordinates and equivalent isotropic displacement parameters (Å^2)

Atoms	Site	*x*	*y*	*z*	U_{eq}[a]	SOF
B	6*a*	0.3233(6)	0	0	0.0167(5)	1
O1	12*c*	0.0479(4)	0.7325(4)	0.02010(9)	0.0267(4)	1
O2	6*a*	0.6007(5)	0	0	0.0382(7)	1
Li1/Al	12*c*	0.0057 (6)	0.3286 (6)	0.0328 (2)	0.020(1)	0.70 (8)/0.09(2)
Li2	6*b*	0.080 (4)	0.161 (8)	0.75	0.04 (1)	0.23 (3)
Li3	12*c*	0.970 (4)	0.340 (4)	0.967 (1)	0.031 (5)	0.25 (2)
Li4	12*c*	0.739(9)	0.395(9)	0.934 (2)	0.03 (1)	0.11(2)
Li5	6*b*	0.377(7)	0.75(1)	0.25	0.03(2)	0.10(3)

[a] $U_{eq} = \frac{1}{3}\sum_i \sum_j U_{ij} a_i^* a_j^* \mathbf{a_i}\mathbf{a_j}$. For Li2–Li5, the displacement parameters presented are U_{iso}.

Table 4
Anisotropic displacement parameters (Å^2)

Atoms	U_{11}	U_{22}	U_{33}	U_{12}	U_{13}	U_{23}
B	0.0163(9)	0.018(1)	0.017(1)	0.0088(7)	0.0003(5)	0.0005(9)
O1	0.0190(7)	0.0202(7)	0.0413(8)	0.0081(6)	0.0049(6)	0.0077(6)
O2	0.0182(7)	0.025(1)	0.074(2)	0.0123(6)	0.0035(6)	0.007(1)
Li1/Al	0.014 (2)	0.017(1)	0.028(2)	0.008(1)	0.0003(9)	0.003(1)

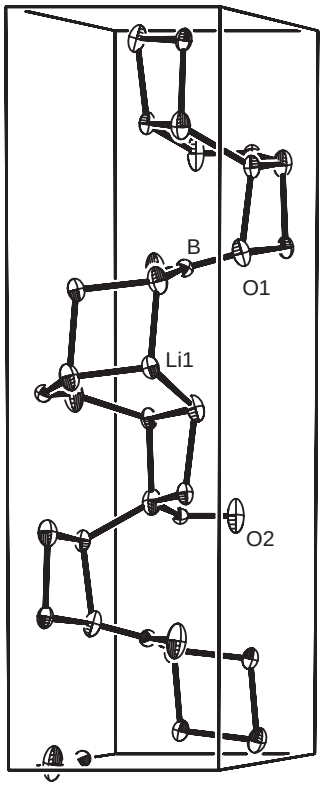

Fig. 2. Unit cell of $Li_{2.46}Al_{0.18}BO_3$ with thermal ellipsoids drawn at 50% probability. Li_2–Li_5 (refined with isotropic thermal parameter) are not shown for clarity.

$Li_{2.46}Al_{0.18}BO_3$ hereafter to keep its electrical neutrality. The unacceptably short Li–Li distances can be explained by the partial occupation of all the Li sites. The details of the refinements are found in Table 1. The atomic positions and anisotropic displacement parameters are listed in Table 3 and Table 4, respectively.

Misinterpretations of the details of a structure often demonstrate themselves with unusual thermal parameters [11]. In our structure model, all the thermal parameters are quite reasonable, and no peculiar ellipsoids are found (see Fig. 2), implying that the structure has been modeled correctly. The selected distances between the cations and anions are presented in Table 5 together with bond valences. For all the cations, the sum of bond valences agrees with the expected values. As can be seen from Table 5, Li1–Li3

Table 5
Selected inter-atomic distances and bond valences

Atoms	Distances (Å)	Bond valences s
Li1–O1	1.898 (3)	0.310
Li1–O2^{i}	1.916 (3)	0.296
Li1–O1^{ii}	1.926 (3)	0.288
Li1–O1^{iii}	2.010 (3)	0.230
ΣS = 1.124		
Li2–O1^{iv}	2.01 (1)	0.227
Li2–O1^{v}	2.01 (1)	0.227
Li2–O2^{vi}	2.03 (2)	0.218
Li2–O2^{vii}	2.03 (2)	0.218
ΣS = 0.890		
Li3–O2^{viii}	1.84 (2)	0.366
Li3–O1^{ix}	1.91 (2)	0.303
Li3–O1^{x}	2.00 (2)	0.239
Li3–O2^{xi}	2.36 (2)	0.090
ΣS = 0.998		
Li4–O1^{xii}	2.01 (4)	0.230
Li4–O1^{xiii}	2.01 (4)	0.230
Li4–O2^{viii}	2.06 (4)	0.201
Li4–O2^{xi}	2.17 (4)	0.149
Li4–O1^{x}	2.19 (3)	0.141
ΣS = 0.951		
Li5–O1^{xiv}	1.96 (4)	0.263
Li5–O1^{xv}	1.96 (4)	0.263
Li5–O2^{xvi}	2.17 (2)	0.148
Li5–O2^{xvii}	2.17 (2)	0.148
ΣS = 0.822		
B–O2	1.360 (4)	1.030
B–O1^{xviii}	1.377 (2)	0.984
B–O1^{ii}	1.377 (2)	0.984
ΣS = 2.998, average B–O = 1.371 Å		

Symmetry codes: (i) $x-1, y, z$; (ii) $1+x-y, 1-y, -z$; (iii) $x, 1+x-y, 1/6-z$; (iv) $-1-x+y, -x, 2/3+z$; (v) $1-y, -x, 5/6-z$; (vi) $y, 1-x+y, 5/6+z$; (vii) $1-x+y, 1-x, 2/3+z$; (viii) $x, y, 1+z$; (ix) $2+x-y, 1-y, 1-z$; (x) $1+x, y, 1+z$; (xi) $1+y, 1-x+y, 5/6+z$; (xii) $y, -x+y, 5/6+z$; (xiii) $1+x-y, 1-y, 1-z$; (xiv) $y, 1+x, 1/3-z$; (xv) $1+x-y, 1+x, 1/6+z$; (xvi) $x-y, x, 1/6+z$; (xvii) $-y, x-y, 1/3+z$; (xviii) $x, y-1, z$.

Table 6
Some relevant bond angles (deg)

O1–Li1–O2^{i}	111.6(1)	O1^{xii}–Li4–O1^{xiii}	98 (2)
O1–Li1–O1^{ii}	115.0(1)	O1^{xii}–Li4–O2^{viii}	161 (2)
O2^{i} –Li1–O1^{ii}	106.9(2)	O1^{xiii}–Li4–O2^{viii}	71 (1)
O1 –Li1–O1^{iii}	101.0(1)	O1^{xii}–Li4–O2^{xi}	69 (1)
O2^{i} –Li1–O1^{iii}	110.6(1)	O1^{xiii}–Li4–O2^{xi}	147 (2)
O1^{ii} –Li1–O1^{iii}	111.8(1)	O2^{viii}–Li4–O2^{xi}	112 (2)
Average	109.5	O1^{xii}–Li4–O1^{x}	102 (2)
		O1^{xiii}–Li4–O1^{x}	100 (2)
O1^{iv}–Li2–O1^{v}	128 (2)	O2^{viii}–Li4–O1^{x}	96 (1)
O1^{iv}–Li2–O2^{vi}	105.90 (9)	O2^{xi}–Li4–O1^{x}	112 (2)
O1^{v}–Li2–O2^{vi}	99.50 (9)		
O1^{iv}–Li2–O2^{vii}	99.50 (9)	O1^{xiv}–Li5–O1^{xv}	101 (3)
O1^{v}–Li2–O2^{vii}	105.90 (9)	O1^{xiv}–Li5–O2^{xvi}	102.6 (7)
O2^{vi}–Li2–O2^{vii}	120(2)	O1^{xv}–Li5–O2^{xvi}	99.4 (6)
Average	110	O1^{xiv}–Li5–O2^{xvii}	99.4 (6)
		O1^{xv}–Li5–O2^{xvii}	102.6 (7)
O2^{viii}–Li3–O1^{ix}	110.9 (9)	O2^{xvi}–Li5–O2^{xvii}	145 (3)
O2^{viii}–Li3–O1^{x}	110.7 (9)	Average	108
O1^{ix}–Li3–O1^{x}	111.4 (8)		
O2^{viii}–Li3–O2^{xi}	113.4 (8)	O2–B–O1^{xviii}	120.3 (1)
O1i^{x}–Li3–O2^{xi}	97.8 (7)	O2–B–O1^{ii}	120.3 (1)
O1^{x}–Li3–O2^{xi}	112.0 (8)	O1^{xviii}–B–O1^{ii}	119.4 (3)
Average	109.4	Average	120.0

Symmetry codes are the same as those in Table 5.

Table 7
Shortest distances between the cation positions (Å)

	B	Li1	Li2	Li3	Li4	Li5
B	>3.3	2.803(4)	2.64(3)	2.81(2)	2.21(4)	2.47(5)
Li1		2.462(6)	1.96(1)	1.17(2)	1.64(4)	1.63(4)
Li2			3.002(7)	1.46(3)	2.15(5)	2.48(1)
Li3				2.33(3)	1.41(4)	1.98(2)
Li4					0.89(7)	2.54(7)
Li5						>3.9

and Li5 are tetrahedrally coordinated while Li4 connects with five O atoms. These LiO_n polyhedra share corners, edges or faces with each other. BO_3 groups are isolated by the LiO_n polyhedra, as in the α $Li3BO_3$ structure. Some relevant bond angles and the shortest distances between cations are given in Table 6 and Table 7, respectively.

3.2. Stacking of the BO_3 group

A projection of the structure along the [210] direction is shown in Fig. 3. The structure consists of six layers of BO_3 groups with Li^+ cations distributing between them. These Li sites are close to each other and a three-dimensional network will result when Li sites within 1.65 Å are connected (see Fig. 3). Another interesting feature of this structure is that Li sites between adjacent BO_3 layers form planar double pentagonal arrangements depicted in Fig. 3. These pentagons are parallel to each other and connect with their counterparts in adjacent layers via Li1–Li3 pairs. The larger and smaller five-membered rings bisect the connections O1–O1 and O2–O2 in adjacent layers, and the sizes of the five-membered rings adjust to the O1–O1 and O2–O2 distances.

3.3. Absolute structure, twinning and disorder

Although the structure has been solved and refined in space group $P6_122$ with quite convincing R-values and reasonable both positional and thermal parameters, the correct absolute structure has not been obtained. For such a compound consisting of only very light elements, it is impossible to discriminate between a pair of enantiomorphic space groups with Mo radiation, as demonstrated by the extremely large deviation of the Flack parameter O(3) [12–14]. In fact, when the structure is ''inverted'', we get exactly the same R-values from the refinement, and all the positions and thermal parameters are kept as reasonable as before.

The disordered structure model could be due to unrecognized twinning. However, for such a space group ($P6_122$ or $P6_522$), the only way of merohedral twinning is the inversion twinning, which is in fact a problem of absolute structure. On the other hand, no hint of pseudo-merohedral twinning was observed in the data collection and structure determination except for the disorder. Moreover, unrecognized pseudo-merohedral twinning usually results in disordered atoms around a site with higher symmetry, which clearly is not the case in our study. The Li+ ions (most likely Li2–Li5) could also be ordered in a supercell of the present one with the disorder being an effect of averaging. As we do not find superstructure reflections, the disordered model represents the compound correctly.

It is quite common to find that Li^+ can be partially substituted by other cations. Li^+ in Li_4SiO_4 can be partially substituted by Al^{3+}, Mg^{2+} and Zn^{2+} to form $Li_{4-3x}Al_xSiO_4$, $Li_{4-2x}Mg_xSiO_4$ or $Li_{4-2x}Zn_xSiO_4$ solid solutions [15–17]. Nevertheless, according to our experimental work in the Li_2O–Al_2O_3–B_2O_3 system [5], the present phase, $Li_{3-x}Al_xBO_3$, seems to be a stoichiometric compound rather than a solid solution. On one hand, this phase cannot be obtained without the presence of Al^{3+}. On the other hand, nearly pure phase can be obtained only when the ratio of Li:Al:B in the starting materials is about 2.4:0.2:1, and an excess or deficiency of Al^{3+} will lead to contamination by other phases. At least, the homogeneity range of this phase is very narrow.

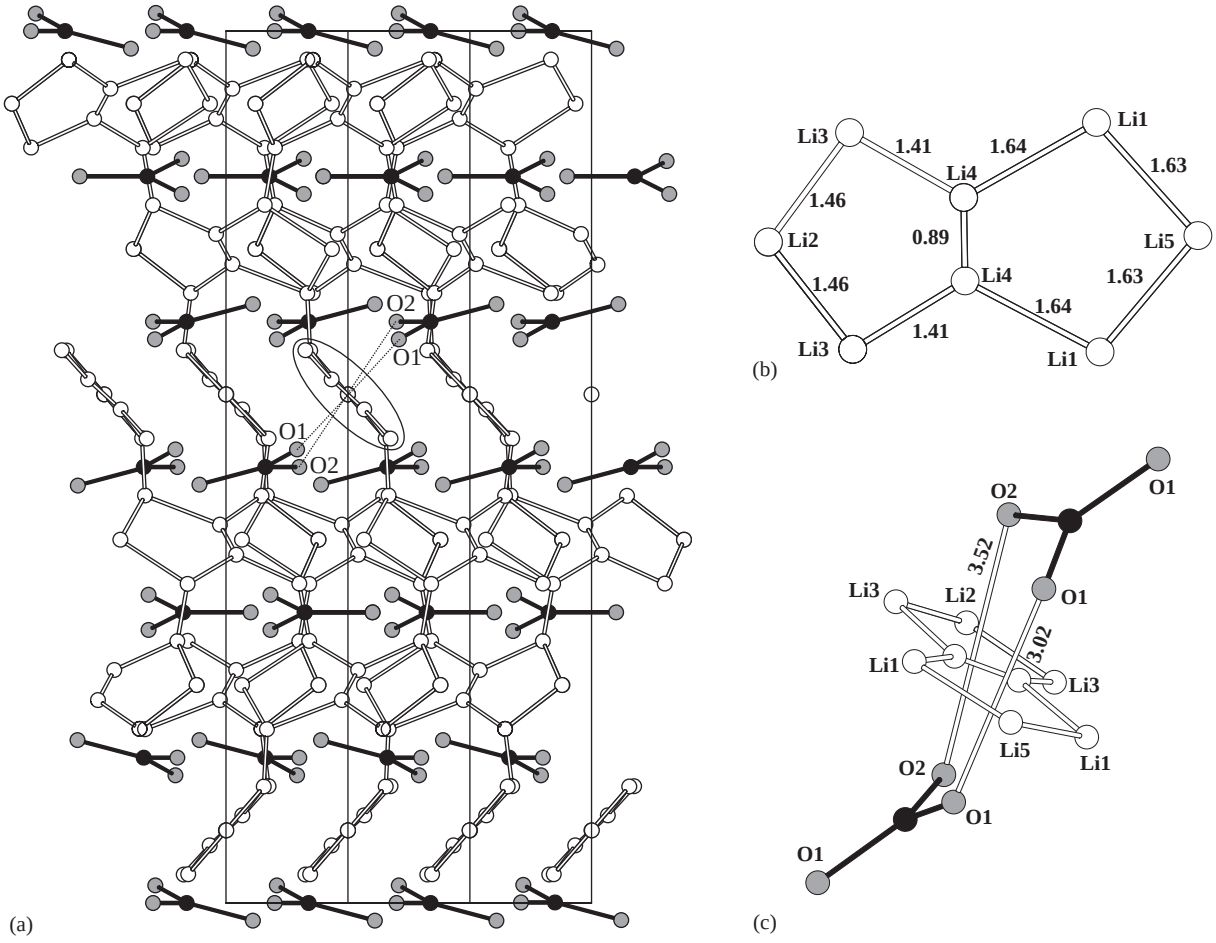

Fig. 3. (a) Structure of $Li_{2.46}Al_{0.18}BO_3$ projected along [210]. Black circles represent B, gray ones O, open ones Li. Solid sticks depict B–O bonds while open sticks highlight the network of Li sites within distance of 1.65 Å. The part marked with a circle in (a) is a double five-membered ring of Li sites, which is shown in (b) in a direction perpendicular to the ring. (c) The large and small five-membered rings bisect connections O1–O1 and O2–O2, respectively. Numbers in (b) and (c) are distances in Angstrom.

Disorder of Li^+ cations is as common as their substitution. Accurate X-ray measurements performed at low temperature (150 K) indicate disorder of Li^+ even in pure (undoped) Li_4SiO_4 [18]. For an Al^{3+}-doped compound, Li^+ disorder is something within our expectation. However, it is really surprising to find that there are five Li sites in the structure and none of them fully occupied. Accordingly, good ionic conductivity is expected for this compound.

3.4. Ionic conduction

The ionic conductivity of the material was investigated by impedance spectroscopy. Impedance spectra showed a depressed high frequency arc and a 45° Warburg-type impedance at low frequencies (see Fig. 4a). The high frequency arc represents the conduction process in the sample interior while the Warburg behavior is assumed to be caused by stoichiometry polarization due to the ionically blocking Au/Pt electrodes. Since a Warburg line is found even at impedance values much higher than the bulk impedance, the DC resistance can be expected to be orders of magnitude larger than the total bulk resistance reflected in the impedance arc. The DC resistance reflects the electron transport, and thus a negligible electron conductivity (compared to the ionic one) can be concluded. The ionic conductivity can therefore be deduced from the size of the high-frequency arc and the corresponding values are shown in Fig. 4b. Reproducible results were obtained in different runs indicating the stability of the sample's microstructure within the chosen temperature range. A significant Li ionic conductivity of ca. 3.5×10^{-7} S/cm and 6×10^{-4} S/cm is found at 100 °C and 300 °C, respectively. The detailed temperature dependence reveals an activation

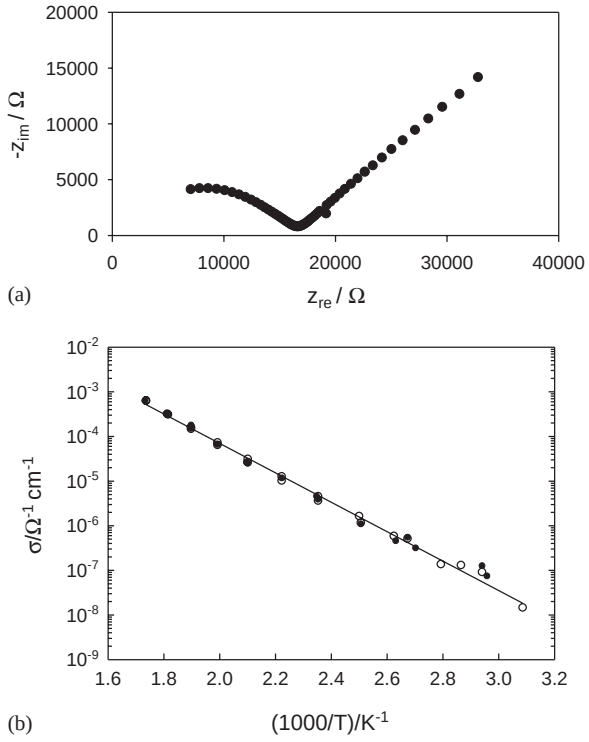

Fig. 4. (a) Impedance spectrum measured at 177 °C between 1 Hz and 1 MHz. (b) Ionic conductivity of $Li_{2.46}Al_{0.18}BO_3$ measured in two different runs (open and closed symbols) each for increasing and decreasing temperature.

energy of 0.65 eV. It should be noted that the compaction process of the sample was not optimized and current detours around pores or current constriction close to imperfect grain-to-grain contacts may considerably increase the resistance compared to a single crystal and might also cause the depression of the bulk arc in the impedance plot. In this case the values of Fig. 4 would only represent the lower limit. The activation energy, however, can be expected not to be affected by complicated current distributions [19].

As mentioned, the measured ionic conductivity of $Li_{3-x}Al_xBO_3$ represents a lower limit due to the non-compact character of the sample. Nevertheless it is two orders of magnitude higher than that of pure Li_3BO_3 and Li_4SiO_4 and comparable to that of the above-mentioned phases after cations substitution [1]. Hence, the Li^+ disorder in the structure is corroborated, however, further experiments are needed to distinguish between the Li^+ vacancy formation due to Al^{3+} substitution and the intrinsic structural disorder of the Li^+ ions.

3.5. Stability range of the phase

Two other phases were found in different runs. Their powder patterns are presented in Fig. 1c and d. The phases identified in Fig. 1b–d are denoted as β, α and γ, respectively. When the starting materials ($0.66Li_2CO_3 \cdot 0.06Al_2O_3 \cdot 0.56H_3BO_3$) were heated at 620 °C for about 3 days, the α phase was obtained. Prolonged annealing of the sample at the same temperature will lead to the β phase, which has been structurally characterized in this study. The powder pattern of the α phase can be indexed with nearly the same unit cell as that of the β phase, but the (003) reflection breaking the extinction law of $P6_122$ or $P6_522$ can be clearly identified in the pattern of the α phase. The relative intensities of the strongest peaks are also different. When the β phase was annealed at slightly higher temperature, e.g., 680 °C, γ phase resulted. The reverse transformation between the β and γ phases was also observed. Because impurities of γ $LiAlO_2$ and β $Li_4B_2O_5$ have been observed in patterns c and d, respectively, α and γ phases could have slightly different composition from the β phase. Unfortunately, we could not find large enough single crystals of the α and γ phases for structure analysis.

Acknowledgement

The authors are very grateful to Dr. C. Hoch and Dr. J. Nuss for internal review, Dr. J. Köhler and Dr. L. Kienle for helpful discussions. This work is financially supported by NSFC under grant number 50372081 and the Max Planck Society.

References

[1] A.P. Rollet, R. Bouaziz, Compt. Rend. 240 (1955) 2417–2419.
[2] R.D. Shannon, B.E. Taylor, A.D. English, T. Berzins, Electrochim. Acta 22 (1977) 783–796.
[3] H. Lehmann, H. Wöckel, Z. Anorg. Allg. Chem. 304 (1960) 121–125.
[4] F. Stewner, Acta Crystallogr. B 27 (1971) 904–910.
[5] M. He, X.L. Chen, B.Q. Hu, T. Zhou, Y.P. Xu, T. Xu, J. Solid State Chem. 165 (2002) 187–192.
[6] L. Wu, X.L. Chen, Q.Y. Tu, M. He, Y. Zhang, Y.P. Xu, J. Alloys Compds. 333 (2002) 154–158.
[7] L. Wu, X.L. Chen, Q.Y. Tu, M. He, Y. Zhang, Y.P. Xu, J. Alloys Compds. 358 (2003) 23–28.
[8] Shelxtl 6.10, Bruker AXS Inc., Madison, Wisconsin, USA, 2000.
[9] A.L. Spek, PLATON. A Multipurpose Crystallographic Tool, Utrecht University, The Netherlands, 2002.
[10] I.D. Brown, D. Altermatt, Acta Crystallogr. B 41 (1985) 244–247.
[11] R.L. Harlow, J. Res. Natl. Inst. Stand. Technol. 101 (1996) 327–339.
[12] H.D. Flack, Acta Crystallogr. A 39 (1983) 876–881.
[13] G. Bernardinelli, H.D. Flack, Acta Crystallogr. A 41 (1985) 500–511.

[14] H.D. Flack, G. Bernardinelli, J. Appl. Cryst. 33 (2000) 1143–1148.
[15] K. Jackowska, A.R. West, J. Mater. Sci. 18 (1983) 2380–2384.
[16] A.R. West, F.P. Glasser, J. Mater. Sci. 5 (1970) 557–565.
[17] A.R. West, F.P. Glasser, J. Mater. Sci. 6 (1971) 1100–1110.
[18] B.H.W.S. de Jong, D. Ellerbroek, A.L. Spek, Acta Crystallogr. B 50 (1994) 511–518.
[19] J. Fleig, J. Maier, J. Electroceramics 1 (1997) 73–89.